Photodeposition of Ag or Pt onto TiO_2 Nanoparticles Decorated on Step Edges of HOPG

James Taing, Ming H. Cheng, and John C. Hemminger*

Department of Chemistry, Center for Solar Energy, University of California Irvine, 334B Rowland Hall, Mail Code 2025, Irvine, California 92697, United States

ABSTRACT Ordered linear arrays of titanium dioxide nanoparticles were fabricated on highly oriented pyrolytic graphite utilizing a step edge decoration method. Ag- or Pt-based nanoparticles were then photodeposited onto the titanium dioxide nanoparticles (~18 nm) to simultaneously verify photocatalytic activity and to demonstrate a viable route to load the titanium dioxide nanoparticles with metals. Scanning electron microscopy and atomic force microscopy determined the morphology, size, and distribution of the particles. X-ray photoelectron spectroscopy confirmed the identity of the titanium dioxide nanoparticles, and transmission electron microscopy showed that some of the particles were rutile single crystals. Energy-dispersive X-ray spectroscopy and X-ray photoelectron spectroscopy determined the chemical composition of the metal-based nanoparticles selectively loaded on the linear arrays of titanium dioxide nanoparticles.

KEYWORDS: HOPG · TiO_2 · step decoration · photodeposition · Ag · Pt

Titanium dioxide (TiO_2) is a proven support for metal, metal oxide, and semiconductor nanoparticles, as well as sensitizers. The composites are relevant to strong metal support interaction (SMSI) studies,[1−7] catalysis, photocatalysis, and energy applications. As a catalyst, Pt,[8] Au,[9] and Cu[9] nanoparticles on TiO_2 facilitate the water−gas shift reaction. As a photocatalyst, Ag nanoparticles on TiO_2 can oxidize[10]/reduce[11,12] organics, demonstrate multicolor photochromism,[13] and act as substrates for surface-enhanced Raman scattering (SERS).[14] Pt nanoparticles on TiO_2 can hydrogenate alkenes and alkynes,[15] decompose carboxylic acids to methane,[16] and enable photoassisted water−gas shift reactions.[17,18] Au nanoparticles on TiO_2 can oxidize carbon monoxide[19,20] and partially oxidize propylene.[20] In terms of energy applications, semiconductor nanoparticles[21] and sensitizers[22−24] on TiO_2 can absorb visible light for solar cells. Ag and Au nanoparticles on TiO_2 can absorb visible light in photoelectrochemical cells *via* surface plasmon resonance.[25] Metal[26,27] and metal oxide[26] nanoparticles on TiO_2 are applicable for synthesizing solar fuels, including Pt on TiO_2 for water splitting.[28−30]

Nanoparticles can be loaded onto TiO_2 *via* a photocatalytic mechanism or from nanoparticle formation in solution followed by adsorption onto the surface. The photocatalytic mechanism offers several advantages including the control of size and distribution of nanoparticles on TiO_2.[31,32] Also, nanoparticles photocatalytically deposited onto TiO_2 show evidence of effective charge transfer compared to deposition from solution.[33] Furthermore, the photocatalytic mechanism allows for the fabrication of multicomponent nanostructures through charge transfer and reduction, ensuring good contact between the components.[34] The photodeposition of nanoparticles onto TiO_2 films from a direct photocatalytic mechanism (heterogeneous photodeposition) cannot be visually distinguished from formation of nanoparticles in solution followed by adsorption onto the surface (homogeneous photodeposition).[16] The two photodeposition mechanisms can be visually distinguished, however, by using an ordered linear array of TiO_2 nanoparticles in place of a TiO_2 film and observing selective deposition onto the TiO_2 nanoparticles *versus* deposition on the entire surface of the substrate. Several types of nanoparticles have been vapor deposited and decorated on steps of highly oriented pyrolytic graphite (HOPG) at room temperature: Ag,[35,36] Ni,[37,38] Bi,[39] Ru,[40] Al,[41] Pt.[42] Ordered linear arrays were obtained with Ag[35,36,43] and Au[44] nanoparticles at elevated substrate temperatures. Previous to the work reported here, there is no clear evidence of ordered linear arrays of Ti or TiO_2 nanoparticles decorating steps of HOPG, although titanium has been vapor deposited on HOPG at room temperature.[45]

In this study, we used physical vapor deposition to grow TiO_2 on HOPG at various temperatures. After decorating steps of HOPG with TiO_2 nanoparticles, we photodeposited

* Address correspondence to jchemmin@uci.edu.

Received for review April 16, 2011 and accepted July 26, 2011.

Published online July 26, 2011
10.1021/nn201396v

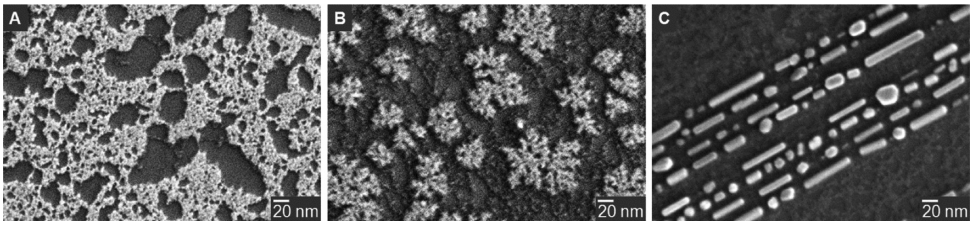

Figure 1. SEM images of TiO_2 on HOPG fabricated with the following conditions: (A) Ta sample holder at 200 °C, deposition thickness 0.7 nm, flux 0.04 nm/min; (B) Ta sample holder at 400 °C, deposition thickness 1.2 nm, flux 0.12 nm/min; (C) Cu sample holder at 550 °C, deposition thickness 1.8 nm, flux 0.3 nm/min. Experiments involving a second thermocouple positioned against the back of the substrate measured temperatures between 800 and 860 °C.

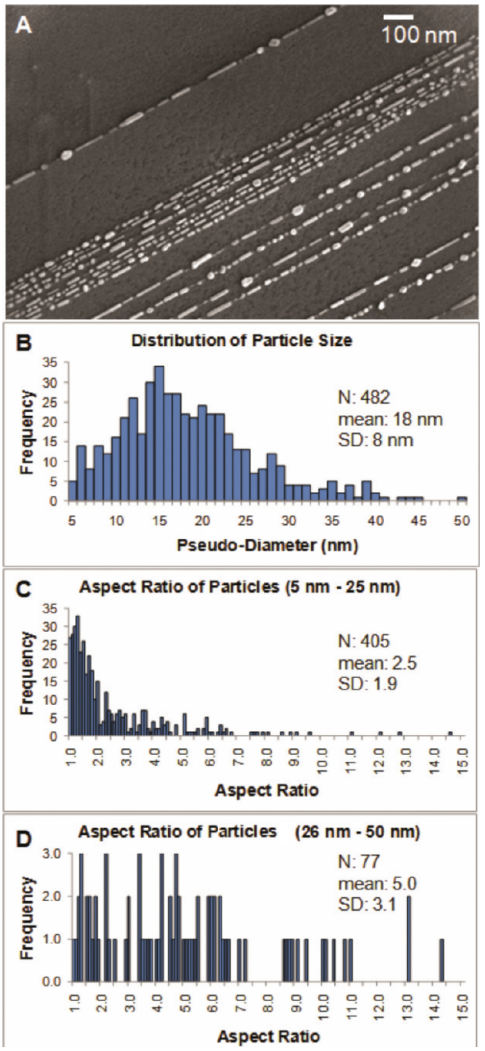

Figure 2. (A) SEM image of TiO_2 nanoparticles decorating steps of HOPG. (B) Size distribution of particles in frame A. (C) Aspect ratio distribution of 5−25 nm particles in frame A. (D) Aspect ratio distribution of 26−50 nm particles in frame A.

Ag- or Pt-based particles onto the TiO_2 nanoparticles. The morphology and distribution of TiO_2 on HOPG and those loaded with Ag- or Pt-based particles were imaged with scanning electron microscopy (SEM) or atomic force microscopy (AFM). The composition and crystal structure of samples were determined from X-ray photoelectron spectroscopy (XPS), energy-dispersive X-ray spectroscopy (EDS), or transmission electron microscopy (TEM).

RESULTS AND DISCUSSION

Physical Vapor Deposition of TiO_2 onto HOPG. Ti was deposited onto HOPG using physical vapor deposition, using a range of substrate temperatures to control the mobility of Ti adatoms and induce step decoration. Upon annealing and oxidation from residual oxygen and water vapor in the evaporator, the resulting morphologies were imaged with SEM. When the sample holder was held at 200 °C during Ti deposition, a thin film formed on the surface of the substrate (Figure 1A). When the sample holder was held at 400 °C during Ti deposition, dendritic structures, with diameters ranging from 20 to 100 nm, grew on the terraces (Figure 1B). At 550 °C, round and rod-shaped nanoparticles exclusively decorated the step edges of the substrate despite increased deposition thickness and flux (Figure 1C). The mean gap size between the particles is 10 nm, and the decoration of step edges extends tens of micrometers.

A zoomed out SEM image of the nanoparticles shows additional decoration of steps (Figure 2A). The mean pseudodiameter of the particles was 18 nm (Figure 2B). The nanoparticles in the region with a high density of steps were smaller (17 nm) than those along the four steps below that were roughly equidistant apart (20 nm). The majority of smaller nanoparticles (5−25 nm) had aspect ratios less than 2 and were thus round or nearly round (Figure 2C). In comparison, the majority of larger nanoparticles (26−50 nm) had larger aspect ratios and were rod-shaped (Figure 2D).

The heights of the round and rod-shaped nanoparticles were compared using AFM (Figure 3A). The line scan of the AFM image measured the height of the round particles to be ~15 nm and roughly double the height of rods (Figure 3B). The height discrepancy may be a result of greater adatom vertical diffusion in the formation of round-shaped particles *versus* lateral diffusion in the formation of rod-shaped particles.

The composition and crystallinity of the nanoparticles were determined with XPS and TEM. In the XPS spectrum, the Ti 2p spin−orbit doublet is associated with Ti $2p_{3/2}$ at a binding energy of 459.7 eV and

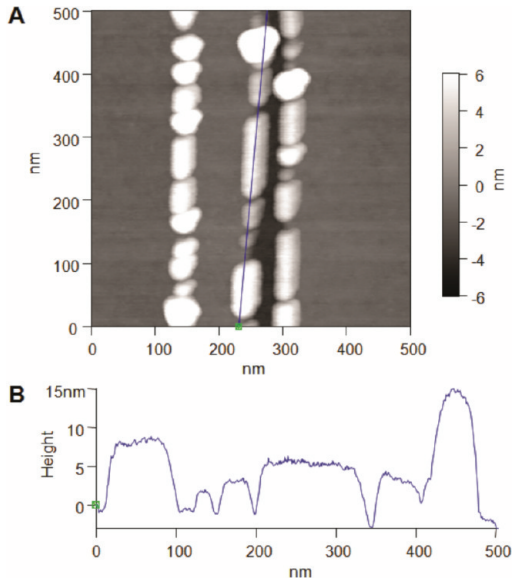

Figure 3. (A) AFM image of TiO_2 nanoparticles decorating steps of HOPG. (B) Line scan of the height of nanoparticles in frame A.

Ti $2p_{1/2}$ at a binding energy of 465.2 eV (Figure 4A). The binding energies agree with TiO_2[46,47] and not of elemental Ti (454.1 eV).[46] Because of the capability to probe a depth of ~10 nm from the surface, which was essentially the full depth of many of the nanoparticles, XPS confirmed complete oxidation of Ti to TiO_2 of many particles.

The TEM image displays a single-crystal nanoparticle with a width of ~25 nm (Figure 4B). A *d* spacing of 3.2 Å was measured from the lattice fringes and fast Fourier transform (FFT) in the inset and corresponds to the 110 plane of rutile TiO_2.[48] The crystal structure disagrees with the most thermodynamically stable phase of TiO_2 based on particle size: anatase (<11 nm), brookite (11−35 nm), and rutile (>35 nm).[49] This discrepancy may be a result of the kinetic growth process of the nanoparticle. Other nanoparticles examined using TEM were also rutile, and many were single crystals.

The decoration of Ti nanoparticles on steps of HOPG required that the substrate remain at elevated temperatures during physical vapor deposition because the supplied thermal energy provided Ti adatoms mobility.[35] With minimal heat, adatoms converged, nucleated, and captured additional adatoms to form dendritic structures on terraces before moving to step edges.[42,44] At higher substrate temperatures, the mobility of the adatoms increased such that the adatoms moved to the step edges, nucleating particles,[50] before nucleation could occur on the terraces. The step edges consist of carbon atoms with fewer coordination numbers,[51] free radicals, alcohols, carbonyls, or carboxlic acids[52] and are more likely to trap the Ti adatoms than the carbon atoms on the terraces. The distribution of smaller particles in areas with a higher density of steps agrees with the theory of steps trapping mobile

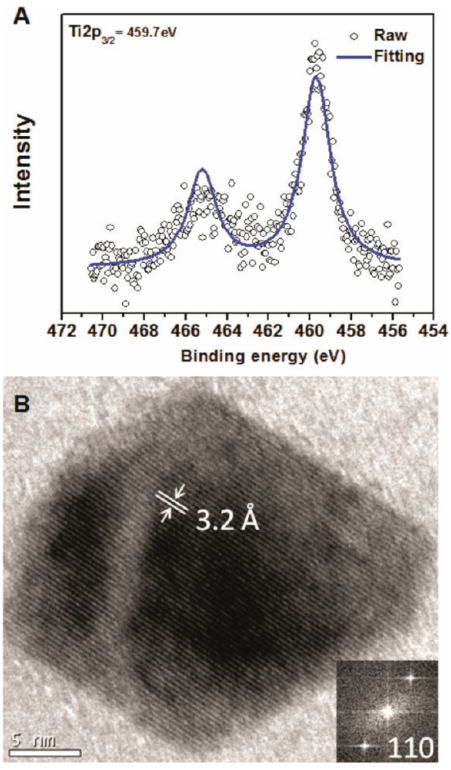

Figure 4. (A) Ti 2p XPS spectrum of TiO_2 nanoparticles on HOPG. (B) TEM image of a TiO_2 nanoparticle single crystal. The inset is the FFT of the lattice fringes and reveals the 110 plane of rutile TiO_2.

adatoms in the vicinity, as in the case of Ag on HOPG.[35] The pressure in the evaporator was not in ultrahigh vacuum (~1×10^{-6} Torr) and signals the presence of residual air. Oxygen and/or water in the residual air oxidized Ti to TiO_2 during physical vapor deposition and 3 h of annealing. Oxidation may have also occurred upon subsequent exposure to ambient air.

The actual temperature required to induce step decoration of the Ti/TiO_2 nanoparticles on HOPG is much higher than the temperature measured on the Cu sample holder, and the substrate radiated bright orange in a dark room. Experiments involving a thermocouple positioned against the back of the substrate measured temperatures between 800 and 860 °C. These temperatures were higher than those observed in the step edge decoration of other elements (Ag,[35,36,43] Ni,[37,38] Bi,[39] Au[44]) above room temperature and agree with the expected relatively strong interaction between Ti and graphene.[53] The interaction, *via* hybridization of Ti adatom 3d orbitals with graphene orbitals, has been described as covalent, and calculations predict a relatively high diffusion barrier (0.5 eV). In the case of Au and graphene, the interaction is described as weaker and calculations predict a lower diffusion barrier (<0.01 eV). The rutile TiO_2 nanoparticles, less than 25 nm, may exhibit enhanced photocatalytic activity compared to larger particles.[54] In addition, single crystals will not suffer

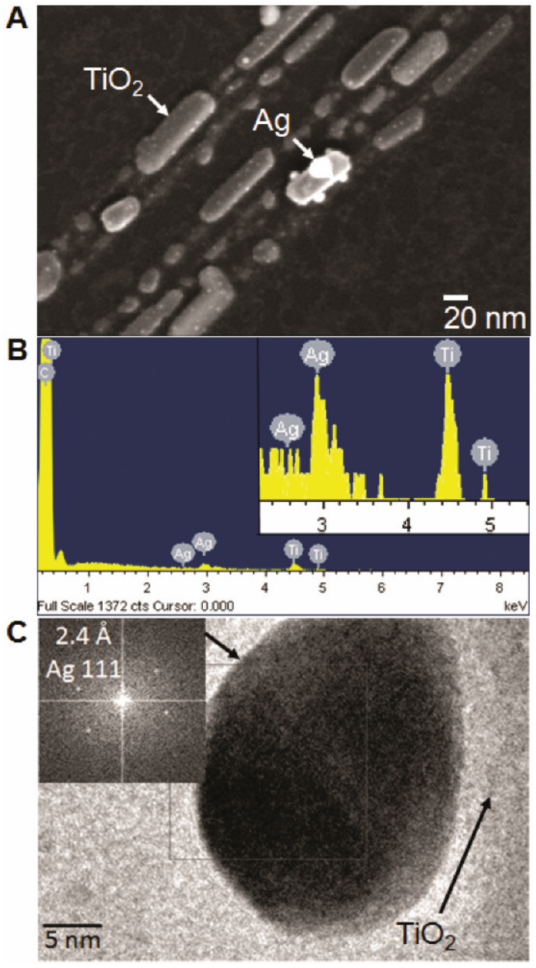

Figure 5. (A) SEM image of Ag nanoparticles selectively photodeposited onto TiO_2 nanoparticles. (B) EDS of the particle labeled "Ag" in frame A. The inset is an expansion of the *y*-axis and shows the relevant signals. (C) TEM image of a Ag nanoparticle on a TiO_2 nanoparticle from the same sample as in frame A. The inset is a FFT of the area of the Ag nanoparticle, marked by a square, and identifies the 111 plane of Ag.

from charge recombination at grain boundaries compared to polycrystalline particles.[55]

Photodeposition of Ag-Based Nanoparticles onto TiO_2 Nanoparticles. The photodeposition of Ag-based nanoparticles onto TiO_2 involved submerging a HOPG substrate, containing steps decorated with TiO_2 nanoparticles, in an aqueous solution of $AgNO_3$ and trisodium citrate and irradiating the sample with ultraviolet (UV) light. The presence of Ag-based nanoparticles selectively deposited onto the TiO_2 nanoparticles would suggest that photodeposition occurred *via* a heterogeneous mechanism. On the other hand, nanoparticles randomly deposited on the HOPG surface would suggest that photodeposition occurred *via* a homogeneous mechanism. As described in the following, we observe predominantly Ag deposition on the TiO_2 nanoparticles, indicating that the major photodeposition mechanism is heterogeneous; however, we did observe some deposition

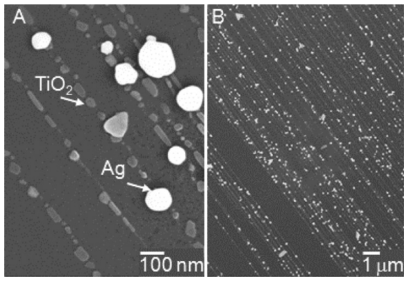

Figure 6. (A) SEM image of Ag particles (>50 nm) on a linear array of TiO_2 nanoparticles. (B) Zoomed out image of frame A.

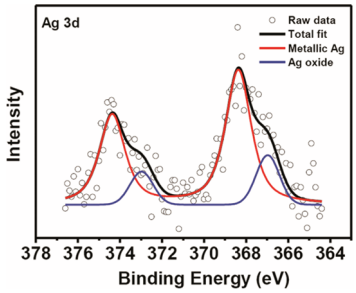

Figure 7. Ag 3d XPS spectrum of a sample consisting of Ag nanoparticles on TiO_2 nanoparticles decorated on steps of HOPG. The binding energies correspond to metallic Ag and Ag oxide.

on the bare HOPG substrate indicative of either homogeneous depositon or electroless deposition. The photodeposition of Ag-based nanoparticles onto TiO_2 nanoparticles was followed by control experiments that tested for electroless deposition.

After photodeposition, an SEM image was taken and shows that many nanoparticles, with diameters less than 5 nm, were dispersed over TiO_2 nanoparticles on the steps of the HOPG substrate (Figure 5A). A few of the particles are larger than 5 nm in width, and EDS confirmed the particle labeled "Ag" is a silver nanoparticle on top of a TiO_2 nanoparticle (Figure 5B). A TEM image shows a nanoparticle on a TiO_2 nanoparticle displayed in a lighter contrast (Figure 5C). From the FFT in the inset, a *d* spacing of 2.4 Å was measured and identified the 111 plane of Ag.[56] Other areas on the sample consisted of Ag particles over 50 nm wide (Figure 6). A Ag 3d XPS spectrum of the sample was deconvoluted to two spin−orbit doublets (Figure 7). The spectrum containing a peak with a binding energy at 368.4 eV corresponds to metallic Ag, whereas the spectrum containing a peak with a binding energy at 367 eV corresponds to Ag oxides.[46] The aforementioned EDS, XPS, and *d* space measurements suggest that the nanoparticles on the TiO_2 nanoparticle(s) in the SEM and TEM images are Ag or Ag oxide.

The selective deposition of Ag-based nanoparticles onto TiO_2 nanoparticles indicates that the photodeposition occurred *via* a heterogeneous mechanism.

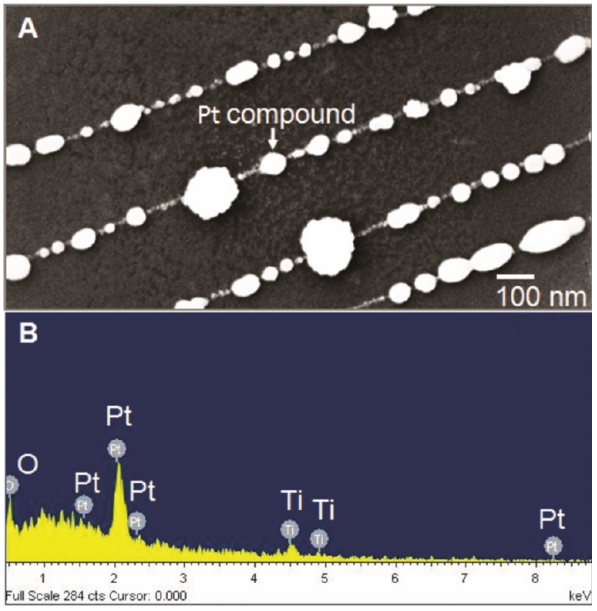

Figure 8. (A) SEM image of a Pt compound selectively photodeposited onto TiO_2 nanoparticles. (B) EDS of the coverage labeled "Pt compound" in frame A.

The rutile TiO_2 nanoparticles (band gap ~3 eV)[57,58] absorbed UV light (365 nm) and generated electrons that reduced the silver cations that adsorbed onto the surface of the TiO_2.[13] Ag^+ can be reduced because of a greater positive standard reduction potential (0.8 V) than Ti^{4+} of TiO_2 (0.0 V).[59] The photogenerated holes oxidized citrate, in the solution, which likely decomposed to acetoacetate and CO_2.[60] The larger Ag nanoparticles were likely a result of diffusion coalescence[61] or Ostwald ripening.[62] Two possible causes may account for the Ag oxide signal in the XPS spectrum: chemical bonding between Ag and oxygen from TiO_2 or growth of an oxide layer upon exposure to ambient air. Some photodeposition experiments resulted in samples containing nanoparticles, several hundred nanometers wide, randomly deposited on the terraces and supports a competing homogeneous photodeposition mechanism. In future experiments, it may be possible to optimize the heterogeneous mechanism by reducing Ag^+ ions adsorbed onto TiO_2 nanoparticles in open air, instead of in a solution,[13,32] or by controlling the adsorption of Ag^+ on the TiO_2 surface.[31]

Upon repeating the photodeposition of Ag experiment using HOPG decorated with TiO_2 nanoparticles, but without UV light, no nanoparticles were selectively deposited onto the TiO_2 nanoparticles. However, a very few sporadic Ag nanoparticles (~100 nm) randomly deposited at the steps and terraces and suggests the minor presence of electroless deposition.

Upon repeating the photodeposition of Ag experiment using HOPG without TiO_2 nanoparticles and without UV light, few Ag nanoparticles, ranging from tens to hundreds of nanometers wide, randomly deposited onto the large steps and terraces. The absence of TiO_2 nanoparticles exposed active sites at the large steps,[52] in addition to defects on the terraces, may have resulted in the greater presence of electroless deposition.

From the control experiments, electroless deposition occurred in the experiments involving the photodeposition of Ag-based nanoparticles and cannot be distinguished from homogeneous photodeposition.

Photodeposition of Pt-Based Nanoparticles onto TiO_2 Nanoparticles. The photodeposition of Pt-based nanoparticles onto TiO_2 was similar to the silver case. A HOPG substrate, containing steps decorated with TiO_2 nanoparticles, was submerged in an aqueous solution containing K_2PtCl_4 and trisodium citrate and irradiated with UV light. We observed Pt-based nanoparticles selectively deposited onto the TiO_2 nanoparticles, indicating that photodeposition occurred *via* a heterogeneous mechanism. The photodeposition of Pt-based nanoparticles onto TiO_2 nanoparticles was followed by control experiments that tested for electroless deposition.

After photodeposition, an SEM image was taken and shows a large coverage on the TiO_2 nanoparticles (Figure 8A). An EDS spectrum of the coverage labeled "Pt compound" shows platinum and oxygen signals that suggests the coverage includes platinum oxides (Figure 8B). From a TEM image of the sample, the coverage consists of an agglomeration of nanoparticles (Figure 9A). The chemical composition of the coverage is further analyzed with XPS (Figure 9B). The Pt 4f spectrum can be deconvoluted to two spin–orbit doublets. The spectrum containing a peak with a binding energy at 74.6 eV corresponds to Pt oxides (PtO, PtO_2), whereas the spectrum containing a

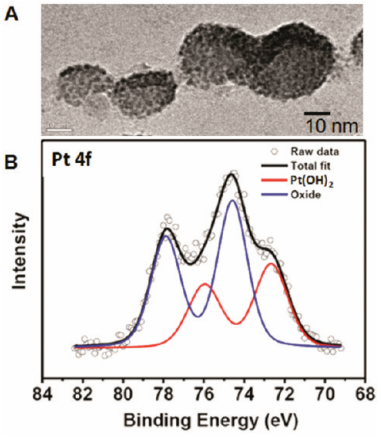

Figure 9. (A) TEM image of a Pt compound covering TiO_2 nanoparticles. (B) Pt 4f XPS spectrum of the same sample as in frame A. The binding energies correspond to Pt oxide and $Pt(OH)_2$.

peak with a binding energy at 72.7 eV corresponds to $Pt(OH)_2$.[46] XPS did not detect elemental Pt, $PtCl_2$, or $PtCl_4$ species.

The Pt−Cl bond in a similar Pt precursor, H_2PtCl_6, is stable in an aqueous solution containing citrate at room temperature.[63] XPS did not detect $PtCl_2$ or $PtCl_4$ and indicates complete decomposition of the Pt precursor. Metallic Pt was also not detected by XPS and may be a consequence of citrate acting more as a stabilizer rather than a reducing agent.[64,65] XPS, however, detected Pt oxides and $Pt(OH)_2$. In previously reported work, PtO_2 and $Pt(OH)_2$ were observed as products of the photocatalytic deposition of Pt onto TiO_2 in a solution using H_2PtCl_6 as the Pt precursor, acetic acid as the electron donor, and NaOH to control pH;[66] the referenced experiment indicates the likely occurrence of a heterogeneous mechanism in our experiment. The presence of oxides may be due to the chemical bonding between Pt and oxygen in TiO_2 or oxidation of Pt nanoparticles. Upon exposure to air and rinsing, Pt nanoparticles could chemisorb oxygen[67−69] and dissociate water,[70,71] causing oxidation and adsorption of hydroxyls. The reactivity for Pt nanoparticles is stronger than bulk because of a greater relative presence of edges and vertices.[72] The complete decomposition of the Pt precursor and selective deposition onto the TiO_2 nanoparticles signify that the deposition of Pt-based nanoparticles onto TiO_2 occurred *via* a heterogeneous mechanism.

Upon repeating the photodeposition of Pt experiment using HOPG decorated with TiO_2 nanoparticles, but without UV light, no nanoparticles were selectively deposited onto the TiO_2 nanoparticles. Furthermore, XPS confirmed no presence of Pt or Pt-based compounds on the sample and indicates the absence of electroless deposition. The control experiment also negates the possibility of simple ligand exchange between chloride, of the Pt precursor, with citrate or hydroxide followed by adsorption onto the TiO_2 nanoparticles.

Upon repeating the photodeposition of Pt experiment using HOPG without TiO_2 nanoparticles and without UV light, no deposition occurred on the substrate. The lack of deposition, confirmed with XPS, again implies the absence of electroless deposition.

From the control experiments, electroless deposition played no role in the experiments involving the photodeposition of Pt-based nanoparticles.

CONCLUSIONS

We fabricated ordered linear arrays of TiO_2 nanoparticles on the steps of HOPG and observed many rutile single crystals. The step edge decoration of Ti, that oxidized to TiO_2 during growth and annealing, required higher substrate temperatures during deposition compared to other elements because of a relatively stronger interaction between Ti and the graphite substrate. The ordered linear arrays of TiO_2 nanoparticles, decorated on steps of HOPG, enabled experiments that can distinguish between a heterogeneous and homogeneous photodeposition. The photodeposition of Ag showed evidence of heterogeneous, homogeneous, and electroless deposition; however, the photodeposition of Pt showed only evidence of heterogeneous photodeposition. The heterogeneous photodeposition of metal-based nanoparticles confirmed the photocatalytic activity of the TiO_2 nanoparticles and demonstrated a viable route to load the TiO_2 nanoparticles with metal nanoparticles.

METHODS

Physical Vapor Deposition of Film, Dendritic Structures, And Ordered Linear Arrays of TiO_2 Nanoparticles. HOPG (ZYB grade, Momentive Performance), freshly cleaved to a thickness of less than 0.25 mm, was used as substrate. The substrates were placed in either a tantalum sample holder or attached at opposite ends with oxygen-free high-temperature copper sample holders (Mo sample holders can work in place of Cu sample holders). The Cu sample holders were used to resistively heat the substrates at higher temperatures not obtainable by the Ta sample holder that was used to radiatively heat the substrates. Both types of sample holders were connected to separate power supplies. The substrates were suspended at a ~57° angle from horizontal and ~11.5 cm above a Ti wire (Alfa Aesar) wrapped inside a W coil (a Ti shot in a tungsten basket can also work). K-type thermocouples were attached to each type of sample holder and respective temperature controllers. The temperature controllers operated the power supplies and maintained temperature on the sample holders *via* a feedback loop.

The substrates were heated above 200 °C in vacuum for a minimum of 2 h to desorb water and organics on the surface before being set to a deposition temperature. Titanium was

deposited on the substrate *via* physical vapor deposition (Edwards 306A coating system), and the amount deposited was measured using a quartz crystal microbalance (Edwards model FTM5). The pressure before the deposition was $\sim 1 \times 10^{-6}$ Torr, and the samples were annealed in vacuum for 3 h after deposition.

Characterization of Ordered Linear Arrays of TiO_2 Nanoparticles. Images of the morphology, lateral dimensions, and distribution of TiO_2 nanoparticles were obtained using a field emission SEM (Zeiss, Ultra Plus) with an InLens detector and an EDS detector (Oxford). The number of particles, lateral surface areas, and aspect ratios were determined using ImageJ image processing software. A pseudodiameter was determined for each particle by equating the lateral surface area of the particle to that of a circle and calculating a diameter. Heights of the nanoparticles were obtained using AFM (Asylum MFP-3D-SA) with silicon tips (Budget Sensors) in AC mode. Chemical identity was determined using XPS (ESCALAB MK II). The instrument is equipped with an Al/Mg twin anode X-ray source and a 150 mm hemispherical electron energy analyzer. Spectra were obtained using Al Kα radiation (1486.6 eV) with a base pressure of 1×10^{-9} Torr. The constant analyzer energy mode was used at constant pass energy for survey scans and narrow scans of 100 and 20 eV, respectively. Binding energies were calibrated using the C 1s peak of HOPG at 284.6 eV as a reference. The crystal structure of the nanoparticles was determined using TEM (FEI/Philips CM-20). The top layers of HOPG, with the nanoparticles, were cleaved with Scotch tape and meticulously placed in copper TEM grids. The *d* spacings of the nanoparticles were measured directly from lattice fringes and FFT using Gatan DigitalMicrograph software.

Photodeposition of Ag- or Pt-Based Nanoparticles onto Ordered Linear Arrays of TiO_2 Nanoparticles. HOPG substrates, with linear arrays of TiO_2 nanoparticles, were placed in a quartz cuvette. For the photodeposition of Ag, the quartz cuvette was filled with an aqueous solution of 0.25 mM $AgNO_3$ (all chemicals purchased from Sigma-Aldrich) and 0.5 mM trisodium citrate. For the photodeposition of Pt, the cuvette was filled with an aqueous solution of 0.25 mM K_2PtCl_4 and 0.5 mM trisodium citrate. The cuvette was slightly tilted such that the surface of the substrate, with the TiO_2 nanoparticles, was pressed against the inside surface of the cuvette due to gravity. A thin film of solution remained present between the surface of the cuvette and the TiO_2 nanoparticles. An optional mask was placed in front of the cuvette such that only half of the sample surface was exposed to incident light for a simultaneous control experiment. The solutions were purged with nitrogen to degas oxygen for 30 min prior to and during the photodeposition of Ag (3 h) or Pt (30 min). In a dark room, 365 nm light from a 200 W Hg lamp was selected by a monochromator and focused onto the sample surface. The sample was repositioned every hour to circulate fresh solution between the cuvette window and sample surface. After photodeposition, the samples were rinsed with deionized water and dried with nitrogen.

Characterization of Ag- or Pt-Based Nanoparticles Photodeposited onto Ordered Linear Arrays of TiO_2 Nanoparticles. The size and distribution of Ag- or Pt-based nanoparticles, photodeposited on linear arrays of TiO_2 nanoparticles, were determined from SEM and TEM images. The chemical composition of the particles was ascertained from EDS and XPS spectra. TEM sample preparation and XPS parameters were the same as those described in the section on characterization of TiO_2 nanoparticles.

Acknowledgment. We thank T. McIntire for AFM assistance and J.-G. Zheng for TEM assistance. Funding was provided by University of California, Irvine Center for Solar Energy and the U.S. Department of Energy, Office of Basic Energy Sciences under Grant DE-FG02-96ER45576.

REFERENCES AND NOTES

1. Tauster, S. J. Strong Metal–Support Interactions. *Acc. Chem. Res.* **1987**, *20*, 389–394.
2. Baker, R. T. K.; Prestridge, E. B.; Garten, R. L. Electron Microscopy of Supported Metal Particles. *J. Catal.* **1978**, *176*, 99–99.
3. Dulub, O.; Hebenstreit, W.; Diebold, U. Imaging Cluster Surfaces with Atomic Resolution: The Strong Metal–Support Interaction State of Pt Supported on TiO_2(110). *Phys. Rev. Lett.* **2000**, *84*, 3646–3649.
4. Pesty, F.; Steinrück, H. P.; Madey, T. E. Thermal Stability of Pt Films on TiO_2(110): Evidence for Encapsulation. *Surf. Sci.* **1995**, *339*, 83–95.
5. Belton, D. N.; Sun, Y. M.; White, J. M. Thin-Film Models of Strong Metal–Support Interaction Catalysts. Platinum on Oxidized Titanium. *J. Phys. Chem.* **1984**, *88*, 1690–1695.
6. Naitabdi, A.; Behafarid, F.; Cuenya, B. R. Enhanced Thermal Stability and Nanoparticle-Mediated Surface Patterning: Pt/TiO_2(110). *Appl. Phys. Lett.* **2009**, *94*, 1–3.
7. Ohyama, J.; Yamamoto, A.; Teramura, K.; Shishido, T.; Tanaka, T. Modification of Metal Nanoparticles with TiO_2 and Metal–Support Interaction in Photodeposition. *ACS Catal.* **2011**, *1*, 187–192.
8. Panagiotopoulou, P.; Christodoulakis, A.; Kondarides, D. I.; Boghosian, S. Particle Size Effects on the Reducibility of Titanium Dioxide and Its Relation to the Water-Gas Shift Activity of Pt/TiO_2 Catalysts. *J. Catal.* **2006**, *240*, 114–125.
9. Rodríguez, J. A.; Evans, J.; Graciani, J.; Park, J. B.; Liu, P.; Hrbek, J.; Sanz, J. F. High Water-Gas Shift Activity in TiO_2(110) Supported Cu and Au Nanoparticles: Role of the Oxide and Metal Particle Size. *J. Phys. Chem. C* **2009**, *113*, 7364–7370.
10. Christopher, P.; Ingram, D. B.; Linic, S. Enhancing Photochemical Activity of Semiconductor Nanoparticles with Optically Active Ag Nanostructures: Photochemistry Mediated by Ag Surface Plasmons. *J. Phys. Chem. C* **2010**, *114*, 9173–9177.
11. Tada, H.; Ishida, T.; Takao, A.; Ito, S. Drastic Enhancement of TiO_2-Photocatalyzed Reduction of Nitrobenzene by Loading Ag Clusters. *Langmuir* **2004**, *20*, 7898–7900.
12. Tada, H.; Teranishi, K.; Inubushi, Y.; Ito, S. TiO_2 Photocatalytic Reduction of Bis(2-dipyridyl)disulfide to 2-Mercaptopyridine by H_2O: Incorporation Effect of Nanometer-Sized Ag Particles. *Chem. Commun.* **1998**, 2345–2346.
13. Ohko, Y.; Tatsuma, T.; Fujii, T.; Naoi, K.; Niwa, C.; Kubota, Y.; Fujishima, A. Multicolour Photochromism of TiO_2 Films Loaded with Silver Nanoparticles. *Nat. Mater.* **2003**, *2*, 29–31.
14. Yang, L. B.; Jiang, X.; Ruan, W. D.; Yang, J. X.; Zhao, B.; Xu, W. Q.; Lombardi, J. R. Charge-Transfer-Induced Surface-Enhanced Raman Scattering on Ag–TiO_2 Nanocomposites. *J. Phys. Chem. C* **2009**, *113*, 16226–16231.
15. Anpo, M.; Aikawa, N.; Kubokawa, Y. Photocatalytic Hydrogenation of Alkynes and Alkenes with Water over TiO_2. Pt-Loading Effect on the Primary Processes. *J. Phys. Chem.* **1984**, *88*, 3998–4000.
16. Kraeutler, B.; Bard, A. J. Heterogenous Photocatalytic Preparation of Supported Catalysts. Photodeposition of Platinum on TiO_2 Powder and Other Substrates. *J. Am. Chem. Soc.* **1978**, *100*, 4317–4318.
17. Sato, S.; White, J. M. Photoassisted Water-Gas Shift Reaction over Platinized TiO_2 Catalyst. *J. Am. Chem. Soc.* **1980**, *102*, 7206–7210.
18. Tsai, S. C.; Kao, C. C.; Chung, Y. W. Photoassisted Water-Gas Shift Reaction over Pt/TiO_2(100). *J. Catal.* **1983**, *79*, 451–461.
19. Valden, M.; Lai, X.; Goodman, D. W. Onset of Catalytic Activity of Gold Clusters on Titania with the Appearance of Nonmetallic Properties. *Science* **1998**, *281*, 1647–1650.
20. Haruta, M. Size- and Support-Dependency in the Catalysis of Gold. *Catal. Today* **1997**, *36*, 153–166.
21. Robel, I.; Kuno, M.; Kamat, P. V. Size-Dependent Electron Injection from Excited CdSe Quantum Dots into TiO_2 Nanoparticles. *J. Am. Chem. Soc.* **2007**, *129*, 4136–4137.
22. O'Regan, B.; Grätzel, M. A Low-Cost, High-Efficiency Solar-Cell Based on Dye-Sensitized Colloidal TiO_2 Films. *Nature* **1991**, *353*, 737–740.
23. Hägglund, C.; Zäch, M.; Kasemo, B. Enhanced Charge Carrier Generation in Dye Sensitized Solar Cells by Nanoparticle Plasmons. *Appl. Phys. Lett.* **2008**, *92*, 1–3.
24. Mora-Seró, I.; Likodimos, V.; Giménez, S.; Martínez-Ferrero, E.; Albero, J.; Palomares, E.; Kontos, A. G.; Falaras, P.; Bisquert,

J. Fast Regeneration of CdSe Quantum Dots by Ru Dye in Sensitized TiO_2 Electrodes. *J. Phys. Chem. C* **2010**, *114*, 6755–6761.
25. Zhao, G.; Kozuka, H.; Yoko, T. Sol-Gel Preparation and Photoelectrochemical Properties of TiO_2 Films Containing Au and Ag Metal Particles. *Thin Solid Films* **1996**, *277*, 147–154.
26. Roy, S. C.; Varghese, O. K.; Paulose, M.; Grimes, C. A. Toward Solar Fuels: Photocatalytic Conversion of Carbon Dioxide to Hydrocarbons. *ACS Nano* **2010**, *4*, 1259–1278.
27. Fu, X. L.; Long, J. L.; Wang, X. X.; Leung, D. Y. C.; Ding, Z. X.; Wu, L.; Zhang, Z. Z.; Li, Z. H.; Fu, X. Z. Photocatalytic Reforming of Biomass: A Systematic Study of Hydrogen Evolution from Glucose Solution. *Int. J. Hydrogen Energy* **2008**, *33*, 6484–6491.
28. Duonghong, D.; Borgarello, E.; Grätzel, M. Dynamics of Light-induced Water Cleavage in Colloidal Systems. *J. Am. Chem. Soc.* **1981**, *103*, 4685–4690.
29. Sayama, K.; Arakawa, H. Effect of Carbonate Salt Addition on the Photocatalytic Decomposition of Liquid Water over $Pt-TiO_2$ Catalyst. *J. Chem. Soc., Faraday Trans.* **1997**, *93*, 1647–1654.
30. Sato, S.; White, J. M. Photodecomposition of Water over Pt/TiO_2 Catalysts. *Chem. Phys. Lett.* **1980**, *72*, 83–86.
31. Zhang, F. X.; Guan, N. J.; Li, Y. Z.; Zhang, X.; Chen, J. X.; Zeng, H. S. Control of Morphology of Silver Clusters Coated on Titanium Dioxide during Photocatalysis. *Langmuir* **2003**, *19*, 8230–8234.
32. Chan, S. C.; Barteau, M. A. Preparation of Highly Uniform Ag/TiO_2 and Au/TiO_2 Supported Nanoparticle Catalysts by Photodeposition. *Langmuir* **2005**, *21*, 5588–5595.
33. Stroyuk, A. L.; Kuchmii, S. Y.; Zhukovskii, M. A.; Smirnova, N. P.; Glebov, E. M.; Grivin, V. P.; Plyusnin, V. F. Effect of the Method of Production of TiO_2/CdS Nanohetero Film Structures on the Effectiveness of Photoinduced Charge Separation. *Theor. Exp. Chem.* **2009**, *45*, 302–307.
34. Tada, H.; Mitsui, T.; Kiyonaga, T.; Akita, T.; Tanaka, K. All-Solid-State Z-Scheme in $CdS-Au-TiO_2$ Three-Component Nanojunction System. *Nat. Mater.* **2006**, *5*, 782–786.
35. Francis, G. M.; Kuipers, L.; Cleaver, J. R. A.; Palmer, R. E. Diffusion Controlled Growth of Metallic Nanoclusters at Selected Surface Sites. *J. Appl. Phys.* **1996**, *79*, 2942–2947.
36. Stabel, A.; Eichhorst-Gerner, K.; Rabe, J. P.; Gonzalez-Elipe, A. R. Surface Defects and Homogeneous Distribution of Silver Particles on HOPG. *Langmuir* **1998**, *14*, 7324–7326.
37. Franc, J.; Bastl, Z. Nickel Evaporation in High Vacuum and Formation of Nickel Oxide Nanoparticles on Highly Oriented Pyrolytic Graphite. X-ray Photoelectron Spectroscopy and Atomic Force Microscopy Study. *Thin Solid Films* **2008**, *516*, 6095–6103.
38. Morant, C.; Soriano, L.; Trigo, J. F.; Sanz, J. M. Atomic Force Microscope Study of the Early Stages of NiO Deposition on Graphite and Mica. *Thin Solid Films* **1998**, *317*, 59–63.
39. McCarthy, D. N.; Robertson, D.; Kowalczyk, P. J.; Brown, S. A. The Effects of Annealing and Growth Temperature on the Morphologies of Bi Nanostructures on HOPG. *Surf. Sci.* **2010**, *604*, 1273–1282.
40. Nielsen, R. M.; Murphy, S.; Strebel, C.; Johansson, M.; Nielsen, J. H.; Chorkendorff, I. A Comparative STM Study of Ru Nanoparticles Deposited on HOPG by Mass-Selected Gas Aggregation *versus* Thermal Evaporation. *Surf. Sci.* **2009**, *603*, 3420–3430.
41. Xiao, W. D.; Kushvaha, S. S.; Wang, X. S. Nucleation and Growth of Aluminum on an Inert Substrate of Graphite. *J. Phys.: Condens. Matter* **2008**, *20*, 1–6.
42. Howells, A. R.; Hung, L.; Chottiner, G. S.; Scherson, D. A. Effects of Substrate Defect Density and Annealing Temperature on the Nature of Pt Clusters Vapor Deposited on the Basal Plane of Highly Oriented Pyrolytic Graphite. *Solid State Ionics* **2002**, *150*, 53–62.
43. Luo, W.; van der Veer, W.; Chu, P.; Mills, D. L.; Penner, R. M.; Hemminger, J. C. Polarization-Dependent Surface Enhanced Raman Scattering from Silver 1D Nanoparticle Arrays. *J. Phys. Chem. C* **2008**, *112*, 11609–11613.
44. Cross, C. E.; Hemminger, J. C.; Penner, R. M. Physical Vapor Deposition of One-Dimensional Nanoparticle Arrays on Graphite: Seeding the Electrodeposition of Gold Nanowires. *Langmuir* **2007**, *23*, 10372–10379.
45. Ma, Q.; Rosenberg, R. A. Interaction of Ti with the (0001) Surface of Highly Oriented Pyrolitic Graphite. *Phys. Rev. B* **1999**, *60*, 2827–2832.
46. Moulder, J. F.; Stickle, W. F.; Sobol, P. E.; Bomben, K. D. *Handbook of X-ray Photoelectron Spectroscopy*; Perkin-Elmer Corporation: Eden Prairie, MN, 1992.
47. Murata, M.; Wakino, K.; Ikeda, S. X-ray Photoelectron Spectroscopic Study of Perovskite Titanates and Related Compounds: An Example of Effect the of Polarization on Chemical Shifts. *J. Electron Spectrosc. Relat. Phenom.* **1975**, *6*, 459–464.
48. Kubiak, P.; Pfanzelt, M.; Geserick, J.; Hormann, U.; Hüsing, N.; Kaiser, U.; Wohlfahrt-Mehrens, M. Electrochemical Evaluation of Rutile TiO_2 Nanoparticles as Negative Electrode for Li-Ion Batteries. *J. Power Sources* **2009**, *194*, 1099–1104.
49. Zhang, H. Z.; Banfield, J. F. Understanding Polymorphic Phase Transformation Behavior During Growth of Nanocrystalline Aggregates: Insights from TiO_2. *J. Phys. Chem. B* **2000**, *104*, 3481–3487.
50. Gates, A. D.; Robins, J. L. Heterogeneous Nucleation on Cleavage Steps 1. Theory. *Surf. Sci.* **1982**, *116*, 188–204.
51. Williams, E. D. Surface Steps and Surface Morphology: Understanding Macroscopic Phenomena from Atomic Observations. *Surf. Sci.* **1994**, *300*, 502–524.
52. Yang, D. Q.; Sacher, E. Interaction of Evaporated Nickel Nanoparticles with Highly Oriented Pyrolytic Graphite: Back-bonding to Surface Defects, As Studied by X-ray Photoelectron Spectroscopy. *J. Phys. Chem. B* **2005**, *109*, 19329–19334.
53. Chan, K. T.; Neaton, J. B.; Cohen, M. L. First-Principles Study of Metal Adatom Adsorption on Graphene. *Phys. Rev. B* **2008**, *77*, 1–12.
54. Anpo, M.; Shima, T.; Kodama, S.; Kubokawa, Y. Photocatalytic Hydrogenation of CH_3CCH with H_2O on Small-Particle TiO_2: Size Quantization Effects and Reaction Intermediates. *J. Phys. Chem.* **1987**, *91*, 4305–4310.
55. Heller, A. Chemical Control of Recombination at Grain Boundaries and Liquid Interfaces: Electrical Power and Hydrogen Generating Photoelectrochemical Cells. *J. Vac. Sci. Technol.* **1982**, *21*, 559–561.
56. Liou, S. H.; Malhotra, S.; Shan, Z. S.; Sellmyer, D. J.; Nafis, S.; Woollam, J. A.; Reed, C. P.; Deangelis, R. J.; Chow, G. M. The Process-Controlled Magnetic Properties of Nanostructured Co/Ag Composite Films. *J. Appl. Phys.* **1991**, *70*, 5882–5884.
57. Reyes-Coronado, D.; Rodríguez-Gattorno, G.; Espinosa-Pesqueira, M. E.; Cab, C.; de Coss, R.; Oskam, G. Phase-Pure TiO_2 Nanoparticles: Anatase, Brookite and Rutile. *Nanotechnology* **2008**, *19*, 1–10.
58. Tang, H.; Prasad, K.; Sanjinès, R.; Schmid, P. E.; Lévy, F. Electrical and Optical Properties of TiO_2 Anatase Thin Films. *J. Appl. Phys.* **1994**, *75*, 2042–2047.
59. Atkins, P.; Paula, J. D. *Physical Chemistry*, 7th ed.; W.H. Freeman and Company: New York, 2002; p 1092.
60. Xue, C.; Métraux, G. S.; Millstone, J. E.; Mirkin, C. A. Mechanistic Study of Photomediated Triangular Silver Nanoprism Growth. *J. Am. Chem. Soc.* **2008**, *130*, 8337–8344.
61. Jak, M. J. J.; Konstapel, C.; van Kreuningen, A.; Verhoeven, J.; Frenken, J. W. M. Scanning Tunnelling Microscopy Study of the Growth of Small Palladium Particles on TiO_2(110). *Surf. Sci.* **2000**, *457*, 295–310.
62. Pillai, Z. S.; Kamat, P. V. What Factors Control the Size and Shape of Silver Nanoparticles in the Citrate Ion Reduction Method? *J. Phys. Chem. B* **2004**, *108*, 945–951.
63. Lin, C. S.; Khan, M. R.; Lin, S. D. Platinum States in Citrate Sols by EXAFS. *J. Colloid Interface Sci.* **2005**, *287*, 366–369.
64. Lin, C. S.; Khan, M. R.; Lin, S. D. The Preparation of Pt Nanoparticles by Methanol and Citrate. *J. Colloid Interface Sci.* **2006**, *299*, 678–685.
65. Henglein, A.; Giersig, M. Reduction of Pt(II) by H_2: Effects of Citrate and NaOH and Reaction Mechanism. *J. Phys. Chem. B* **2000**, *104*, 6767–6772.
66. Vorontsov, A. V.; Savinov, E. N.; Jin, Z. S. Influence of the Form of Photodeposited Platinum on Titania upon Its

Photocatalytic Activity in CO and Acetone Oxidation. *J. Photochem. Photobiol., A* **1999**, *125*, 113–117.
67. Gland, J. L.; Korchak, V. N. The Adsorption of Oxygen on a Stepped Platinum Single Crystal Surface. *Surf. Sci.* **1978**, *75*, 733–750.
68. Gland, J. L. Molecular and Atomic Adsorption of Oxygen on the Pt(111) and Pt(S)-12(111) X(111) Surfaces. *Surf. Sci.* **1980**, *93*, 487–514.
69. Ducros, R.; Merrill, R. P. The Interaction of Oxygen with Pt(110). *Surf. Sci.* **1976**, *55*, 227–245.
70. Fisher, G. B.; Sexton, B. A. Identification of an Adsorbed Hydroxyl Species on the Pt(111) Surface. *Phys. Rev. Lett.* **1980**, *44*, 683–686.
71. Seitsonen, A. P.; Zhu, Y. J.; Bedurftig, K.; Over, H. Bonding Mechanism and Atomic Geometry of an Ordered Hydroxyl Overlayer on Pt(111). *J. Am. Chem. Soc.* **2001**, *123*, 7347–7351.
72. Han, B. C.; Miranda, C. R.; Ceder, G. Effect of Particle Size and Surface Structure on Adsorption of O and OH on Platinum Nanoparticles: A First-Principles Study. *Phys. Rev. B* **2008**, *77*, 1–9.